Research Square

Preprints are preliminary reports that have not undergone peer review.
They should not be considered conclusive, used to inform clinical practice,
or referenced by the media as validated information.

Nuclear proteomics identifies TEAD4 as an IFN-γ-responsive regulator of pathogenic synovial fibroblast programs

Tetsuya Saito

saito.rheu@tmd.ac.jp

Department of Rheumatology, Graduate School of Medical and Dental Sciences, Institute of Science Tokyo https://orcid.org/0009-0003-7241-6662

Motohiko Sato

Kenta Horie

https://orcid.org/0000-0003-4175-1014

Takahiro Nakahara

Rihan Da

Shiyao Li

Akio Yamamoto

Seiji Noda

Tadashi Hosoya

Yasuhiro Takahara

Kazutaka Sugimoto

Kentaro Endo

Tokyo Medical and Dental University

Hideyuki Koga

Ichiro Sekiya

Tokyo Medical and Dental University https://orcid.org/0000-0002-6331-722X

Eiryo Kawakami

Chiba University https://orcid.org/0000-0001-9955-4342

Shinsuke Yasuda

Tokyo Medical and Dental University https://orcid.org/0000-0001-6171-2077

Article

Keywords: Difficult-to-treat rheumatoid arthritis, Synovial fibroblast subset, Data- independent acquisition mass spectrometry, YAP/TAZ, TEAD

Posted Date: November 10th, 2026

DOI: https://doi.org/10.21203/rs.3.rs-11191053/v1

License: This work is licensed under a Creative Commons Attribution 4.0 International License.
Read Full License

Additional Declarations: Yes there is potential Competing Interest. TS received research funding from Eli Lilly, speaking fees from Abbvie, Asahi Kasei Pharma, Chugai Pharmaceutical, Eisai, Eli Lilly, GlaxoSmithKline, Mitsubishi Tanabe Pharma, Ono Pharmaceutical, Taisho Pharmaceutical, and Astellas Pharma. SY received research funding from Asahi Kasei Pharma, Ayumi Pharmaceutical Corporation, Chugai Pharmaceutical, Nippon Boehringer Ingelheim Co., Ltd, and Taisho Pharmaceutical Co., Ltd, speaking fees from Abbvie, Asahi Kasei Pharma, Chugai Pharmaceutical, Eisai, Eli Lilly, GlaxoSmithKline, Mitsubishi Tanabe Pharma, and Ono Pharmaceutical, consultant fee from Eisai, ImmunoForge, Novartis and Otsuka seiyaku.

Nuclear proteomics identifies TEAD4 as an IFN-γ-responsive regulator of pathogenic synovial fibroblast programs

Tetsuya Saito[1*], Motohiko Sato[1], Kenta Horie[2,3,4], Takahiro Nakahara[1], Rihan Da[1], Shiyao Li[1], Akio Yamamoto[1], Seiji Noda[1], Tadashi Hosoya[1], Yasuhiro Takahara[5], Kazutaka Sugimoto[6], Kentaro Endo[7], Hideyuki Koga[8], Ichiro Sekiya[7], Eiryo Kawakami[2,3,4,9], Shinsuke Yasuda[1*]

1) Department of Rheumatology, Graduate School of Medical and Dental Sciences, Institute of Science Tokyo (IST), Tokyo, Japan
2) Department of Artificial Intelligence Medicine, Graduate School of Medicine, Chiba University, Chiba, Japan
3) Predictive Medicine Special Project (PMSP), RIKEN Center for Integrative Medical Sciences (IMS), RIKEN, Yokohama, Kanagawa, Japan
4) Institute for Advanced Academic Research (IAAR), Chiba University, Chiba, Japan.
5) Department of Orthopedic Surgery, Nippon Kokan Fukuyama Hospital, Hiroshima, Japan
6) Department of Orthopedics, Sonodakai Joint Replacement Center Hospital, Tokyo, Japan
7) Center for Stem Cell and Regenerative Medicine, Institute of Science Tokyo (IST), Tokyo, Japan
8) Department of Joint Surgery and Sports Medicine, Graduate School of Medical and Dental Sciences, Institute of Science Tokyo (IST), Tokyo, Japan
9) Division of Applied Mathematical Science, RIKEN Center for Interdisciplinary Theoretical and Mathematical Sciences, RIKEN, Yokohama, Kanagawa, Japan

*Corresponding author: Shinsuke Yasuda and Tetsuya Saito

Email: syasuda.rheu@tmd.ac.jp and saito.rheu@tmd.ac.jp

Author Contributions: TS, EK and SY designated the research. TS, MT, KH, TN, RD and ST performed experiments. KH and EK performed statistical analyses. TS, KH and SY analyzed and interpreted the data. TS, TH and SY drafted the manuscript. AY, SN, YT, KS, KN, HK and IK provided synovial tissues from patients. All authors contributed to the discussion and had opportunities to revise the manuscript.

Competing Interest Statement: TS received research funding from Eli Lilly, speaking fees from Abbvie, Asahi Kasei Pharma, Chugai Pharmaceutical, Eisai, Eli Lilly, GlaxoSmithKline, Mitsubishi Tanabe Pharma, Ono Pharmaceutical, Taisho

Pharmaceutical, and Astellas Pharma. SY received research funding from Asahi Kasei Pharma, Ayumi Pharmaceutical Corporation, Chugai Pharmaceutical, Nippon Boehringer Ingelheim Co., Ltd, and Taisho Pharmaceutical Co., Ltd, speaking fees from Abbvie, Asahi Kasei Pharma, Chugai Pharmaceutical, Eisai, Eli Lilly, GlaxoSmithKline, Mitsubishi Tanabe Pharma, and Ono Pharmaceutical, consultant fee from Eisai, ImmunoForge, Novartis and Otsuka seiyaku.

Keywords: Difficult-to-treat rheumatoid arthritis, Synovial fibroblast subset, Data-independent acquisition mass spectrometry, YAP/TAZ, TEAD.

This PDF file includes:

Main Text
Figures 1 to 6 (Supplementary Figures 1 to 4)
Supplementary Tables 1 to 2

Abstract

Difficult-to-treat rheumatoid arthritis (D2T RA) remains a major unmet clinical challenge despite advances in targeted therapies. Recent single-cell and spatial transcriptomic studies identified synovial fibroblast (SF) subsets associated with multidrug-resistant disease states. Transcriptome-based inference approaches have been used to further characterize pathogenic fibroblast subsets by identifying candidate master transcriptional regulators. However, their accuracy is limited by the context-dependent relationship between transcription factors and their target genes. Here, we applied nuclear proteomics using data-independent acquisition mass spectrometry (DIA-MS) to identify transcription factors regulated in cytokine-stimulated rheumatoid arthritis synovial fibroblasts (RASFs). Nuclear DIA-MS identified TEAD4 as a transcription factor selectively induced by IFN-γ signaling. Transcriptomic and functional analyses demonstrated that TEAD4 regulates gene programs associated with multidrug-resistant fibroblast subsets, including TGF-β-associated fibroblast activation programs. Comparative perturbation analyses showed that TEAD family members exhibit both redundant and distinct functions and regulate transcriptional programs that only partially overlap with those controlled by YAP/TAZ. Pharmacologic inhibition of TEAD activity suppressed fibroblast proliferation and migration in vitro and attenuated arthritis severity in the collagen-induced arthritis model without impairing antigen-specific immune responses. Together, these findings identify TEAD signaling as a therapeutically targetable pathway in rheumatoid arthritis and provide a mechanistic framework linking inflammatory and profibrotic fibroblast activation.

Main Text

Introduction

Rheumatoid arthritis (RA) is a chronic autoimmune disease characterized by synovial inflammation and destructive joint remodeling, driven by complex interactions between immune and stromal cells, including synovial fibroblasts (SFs)(1–3). Molecularly targeted disease-modifying antirheumatic drugs (DMARDs), including biologic and targeted synthetic DMARDs, have substantially improved clinical outcomes. However, approximately 20% of patients remain refractory to multiple therapies, a condition defined as difficult-to-treat rheumatoid arthritis (D2T RA)(4). Identifying the molecular mechanisms underlying D2T RA and developing new therapeutic strategies remain major unmet clinical needs.

Single-cell RNA sequencing (scRNA-seq) and spatial transcriptomic analyses have revealed marked heterogeneity among rheumatoid arthritis synovial fibroblasts (RASFs), which comprise anatomically and functionally distinct subsets(5–10). RASFs are broadly classified into THY1^- lining and THY1^+ sublining populations, the latter including transcriptionally distinct subsets such as THY1^+CD34^+, THY1^+DKK3^+, THY1^+HLA-DR^high, THY1^high, THY1^+GAS6^+, THY1^+ITGA5^+, and THY1^+COMP^high fibroblasts. These subsets are shaped by inflammatory cytokines, including TNF-α, IL-1β, IFN-γ,

and TGF-β, together with developmental pathways such as Notch and Wnt(8, 11, 12).

Recent studies, including the R4RA trial, have highlighted the contribution of specific fibroblast subsets to treatment resistance(13, 14). Gene signatures associated with THY1+DKK3+ and related fibroblast populations are enriched in patients who fail multiple biologic therapies. More recently, spatial transcriptomic analyses identified COMP^high fibroblasts that localize to perivascular niches, exhibit persistent TGF-β activation, and persist despite immune cell depletion(10). In addition, ITGA5+ fibroblasts have been shown to integrate inflammatory and profibrotic signals, including IFN-γ and TGF-β. Together, these observations support a fibroblast-intrinsic mechanism underlying persistent disease in D2T RA. RASFs exhibit tumor-like properties, including enhanced proliferation, migration, extracellular matrix remodeling, and sustained production of cytokines and chemokines(3). Experimental studies have demonstrated distinct roles for lining and sublining fibroblasts in tissue destruction and inflammation(15). Although current therapies primarily target immune cells, fibroblast-directed approaches such as cyclin-dependent kinase inhibition have recently emerged as promising therapeutic strategies(16–18). Nevertheless, additional molecular targets that selectively regulate pathogenic fibroblast states remain to be identified.

The Hippo pathway regulates cell proliferation and survival through the transcriptional coactivators YAP and TAZ, which interact with TEAD transcription factors to regulate genes including ANKRD1, CCN1, and CTGF(19, 20). In fibroblasts, the YAP/TAZ-TEAD complex mediates mechanotransduction in response to extracellular matrix stiffness and TGF-β signaling(20, 21). Although YAP/TAZ signaling contributes to fibroblast activation and arthritis pathogenesis(22–24), the role of individual TEAD family members in pathogenic fibroblast states remains incompletely understood.

Identifying transcriptional regulators that govern pathogenic fibroblast states remains challenging. We previously identified ARID5B and GLI3 as transcription factors enriched in pathogenic RASF subsets and demonstrated that both functioned as negative regulators of fibroblast pathogenicity, indicating that transcription factors highly expressed in pathogenic subsets are not necessarily drivers of disease states(25, 26). Furthermore, inference-based approaches using transcriptomic data, including SCENIC, VIPER, and weighted parametric gene set analysis (wPGSA), estimate transcription factor activity indirectly from downstream gene expression and are limited by context-dependent transcriptional regulation (27, 28). Data-independent acquisition mass spectrometry (DIA-MS) enables direct quantification of transcription factors within the nuclear proteome and therefore provides a complementary approach for identifying transcriptional regulators functionally associated with pathogenic fibroblast programs(29, 30).

In the present study, we applied nuclear DIA-MS to RASFs stimulated with a cytokine combination consisting of TNF-α, IL-1β, IFN-γ, and TGF-β1 that recapitulates key inflammatory and profibrotic signals present in the RA

synovium(8, 9, 31–33). We identified TEAD4 as an IFN-γ-responsive transcription factor associated with pathogenic fibroblast programs. Functional genomic and pharmacologic analyses further demonstrate that TEAD signaling contributes to transcriptional programs associated with treatment-resistant fibroblast states and represents a potential therapeutic target in rheumatoid arthritis.

Results

Nuclear proteomics identifies TEAD4 as an IFN-γ-responsive transcription factor in pathogenic synovial fibroblasts. To identify transcriptional regulators associated with pathogenic RASF states, we performed quantitative proteomic analysis of nuclear extracts from bulk RASFs treated with a combination of four cytokines (referred to as "4mix") previously implicated in pathogenic RASF activation(8–10): TNF-α, IL-1β, IFN-γ, and TGF-β1 (Fig. 1*A*). By analyzing nuclear extracts rather than whole-cell lysates, we sought to identify transcription factors regulated not only at the transcriptional level but also through post-translational mechanisms, including nuclear translocation and protein turnover. Quantitative DIA-MS identified 208 transcription factors significantly altered by 4mix stimulation, including 87 upregulated and 111 downregulated factors (Fig. 1*B*, Fig. S1*A*). Among the upregulated TFs were canonical regulators associated with individual cytokine pathways, including NFKB1/2 and REL (TNF-α), FOSL1, JUNB, BATF2/3, and CEBPB (IL-1β), IRF1 (IFN-γ), and SMAD1 (TGF-β). In addition, transcription factors previously implicated in RASF pathogenicity, including MTF1(33), RUNX1(33, 34), ETS1(35), and BACH1(36), were also identified (Fig. 1*B*), demonstrating the ability of nuclear DIA-MS to identify disease-relevant transcription factors in activated RASFs. We next focused on TEAD4, a member of the TEAD family (TEAD1-4), because YAP/TAZ-TEAD signaling is a key mediator of TGF-β-dependent mechanotransduction in fibroblasts (Fig. 1*C*)(19, 37). In fibroblasts, the YAP/TAZ–TEAD complex mediates mechanotransduction in response to extracellular matrix stiffness and TGF-β signaling, which has been implicated in the differentiation of D2T RA-associated fibroblast subsets(9, 10, 20). Re-analysis of the DIA-MS data revealed that TEAD1, TEAD3, and TEAD4 were detectable in RASFs, whereas TEAD2 was not (Fig. 1*D*). Notably, only TEAD4 was consistently upregulated by 4mix stimulation, while YAP, TAZ, LATS1, and LATS2 showed little change (Fig. 1*D*). Induction of TEAD4 was further confirmed by immunoblotting (Fig. 1*E*).

To further evaluate TEAD4 activity in activated RASFs, we performed RNA-seq followed by wPGSA of RASFs treated with 4mix or vehicle for 24 h (Fig. 1*F*, Fig. S1*A*, *B*). Because wPGSA estimates transcription factor activity using transcriptomic data and publicly available ChIP-seq datasets(27), we used it as a complementary approach to compare with nuclear proteomic findings. 4mix induced genes associated with inflammatory pathways relevant to RA, including TNF, JAK-STAT, and NF-κB signaling (Fig. S2*A*, *B*). Consistent with the DIA-MS results, wPGSA identified increased activities of TEAD4 and TEAD1 together with IRFs, NF-κB, AP-1, and STAT family members (Fig. 1*F*). We next applied wPGSA

to published scRNA-seq data from RA synovial tissues obtained during active disease and remission (Fig. 1*G*). The dataset comprised five RASF subsets: lining, HLA^high, THY1^high, GAS6^+, and CD34^+ fibroblasts(7). The THY1^high subset overlaps with previously described DKK3^+ and COMP^high fibroblast populations associated with treatment resistance(7, 10, 13). TEAD4 and TEAD1 activities were significantly increased ($q < 0.05$) in multiple fibroblast subsets from active RA, with the highest TEAD4 activity observed in THY1^high fibroblasts (Fig. 1*G*). SMAD and AP-1 activities were also enriched in this subset, consistent with coordinated regulation of inflammatory and profibrotic transcriptional programs(20, 38). Collectively, these findings identify TEAD4 as an IFN-γ-responsive transcription factor associated with pathogenic fibroblast subsets and support its potential role in regulating multidrug-resistant fibroblast programs in rheumatoid arthritis.

TEAD4 is induced by IFN-γ through the JAK/STAT pathway

Given that TEAD4 protein levels were increased following 4mix stimulation, we next sought to determine which cytokine was responsible for its induction. Treatment of RASFs with TNF-α, IL-1β, or TGF-β1 alone had little effect, whereas IFN-γ alone, either alone or in combination with other cytokines, markedly increased TEAD4 protein expression (Fig. 2*A*). To determine whether TEAD4 induction occurred at the transcriptional level, we measured TEAD4 mRNA expression at early (4 h) and late (24 h) time points. Consistent with the immunoblotting results, TEAD4 mRNA was rapidly and robustly induced by IFN-γ in the presence or absence of the other cytokines (Fig. 2*B*), suggesting transcriptional regulation by IFN-γ signaling.

To further investigate the mechanism underlying IFN-γ-mediated TEAD4 induction, we analyzed publicly available STAT1 ChIP-seq datasets from ChIP-Atlas (https://chip-atlas.org)(39). These analyses revealed clear STAT1 binding at the TEAD4 promoter in IFN-γ-stimulated cells, including SET-2, Huh-7, and HeLa cells (Fig. S2).

We next examined whether TEAD4 induction depended on the canonical IFN-γ receptor (IFNGR)-JAK1/2-STAT1 pathway using clinically approved JAK inhibitors employed in RA treatment (Fig. 2*C*). TEAD4 mRNA induction by 4mix was dose-dependently suppressed by pan-JAK and JAK1/2-selective inhibitors, including tofacitinib, baricitinib, and upadacitinib(40), whereas the JAK1-selective inhibitor filgotinib showed only modest effects(40). This inhibition profile closely resembled that of IRF1, a well-established STAT1 target gene, but differed from IL6, whose expression was largely unaffected. Together, these findings support regulation of TEAD4 through the IFNGR-JAK1/2-STAT1 signaling pathway.

Finally, we examined TEAD4 expression in RA synovial tissue. Recent spatial transcriptomic studies have demonstrated nuclear pSTAT1 activation in both THY1^- lining and THY1^+ sublining fibroblasts located adjacent to IFN-γ-producing CD8^+ T cells and NK cells(8). Consistent with these observations, immunohistochemistry demonstrated nuclear TEAD4 expression in spindle-shaped cells within both the lining and sublining layers of RA synovium, whereas expression was minimal in osteoarthritis (OA) tissues (Fig. 2*D*). TEAD4 was also

detected in endothelial and mural cells but was largely absent from lymphocytes. Together, these findings identify TEAD4 as an IFN-γ-responsive transcription factor expressed in activated synovial fibroblasts within RA synovial tissue.

TEAD4 contributes to the active state of pathogenic RASF subsets

To investigate the functional significance of TEAD4 in pathogenic RASF subsets, we performed RNA-seq analysis of RASFs transfected with siRNA targeting TEAD4 (siTEAD4) or control siRNA (siCtrl), followed by stimulation with 4mix for 24 h. TEAD4 knockdown resulted in the downregulation of 585 genes and upregulation of 241 genes ($|\log2FC| > 1.0$, $q < 0.05$) (Fig. 3*A*). Among canonical YAP/TAZ/TEAD target genes, ANKRD1 was markedly reduced following TEAD4 knockdown, whereas CCN1 and CTGF were less affected, suggesting that TEAD4 preferentially regulates a subset of YAP/TAZ/TEAD-responsive genes in RASFs. KEGG pathway analysis demonstrated enrichment of downregulated genes in pathways associated with fibroblast activation, including focal adhesion, PI3K-Akt, mTOR, MAPK, and TGF-β signaling (Fig. 3*B*). In contrast, genes involved in cytosolic DNA sensing and several metabolic pathways were modestly upregulated (Fig. 3*B*).

Because TEAD4 activity was enriched in pathogenic fibroblast subsets (Fig. 1*G*), we next examined the effect of TEAD4 knockdown on transcriptional signatures associated with treatment-resistant fibroblast states (Fig. 3*C*). Gene signatures previously associated with treatment resistance in the R4RA trial(13), together with marker genes of DKK3^+ and THY1^high fibroblast subsets(6, 7), were significantly suppressed following TEAD4 knockdown (Fig. 3*C*). To validate these findings, we performed qPCR using an independent siRNA targeting TEAD4. These experiments confirmed suppression of 4mix-induced ANKRD1 expression (Fig. 3*D*). TEAD4 knockdown also significantly reduced expression of COMP and PRELP, markers associated with multidrug-resistant fibroblast subsets(10, 13), together with additional genes implicated in fibroblast pathogenicity, including TGFBR2(9, 10) and IL1R1(41). Taken together, these findings indicate that IFN-γ-inducible TEAD4 regulates transcriptional programs associated with pathogenic and multidrug-resistant RASF subsets and support a role for TEAD4 in fibroblast activation associated with treatment-resistant rheumatoid arthritis.

TEAD1, TEAD3, and TEAD4 exhibit redundant and distinct functions and differentially regulate transcriptional programs relative to YAP/TAZ

RNA-seq analysis following TEAD4 knockdown suggested that additional TEAD family members contribute to Hippo-associated transcriptional programs in RASFs. We therefore examined the roles of TEAD1, TEAD3, and TEAD4 individually and in combination. Western blotting using a pan-TEAD antibody revealed two major bands around 50 kDa in RASFs. The upper and lower bands were selectively depleted following siTEAD1 and siTEAD3, respectively, whereas a TEAD4-specific antibody confirmed efficient depletion of TEAD4 (Fig. 4*A*).

We next examined the effects of individual and combinatorial knockdown of TEAD isoforms on canonical YAP/TAZ/TEAD target genes (Fig. 4*B*). Even among well-established target genes, the contribution of individual TEAD isoforms differed. ANKRD1 expression was almost completely abolished by siTEAD4 alone, with

partial additive effects of siTEAD1. In contrast, effective suppression of CCN1 required simultaneous knockdown of all TEAD isoforms, indicating substantial functional redundancy. CTGF expression was predominantly regulated by TEAD1 and TEAD3, whereas TEAD4 made a more modest contribution. We also examined inflammatory mediators. Previous studies have implicated the YAP/TAZ-TEAD complex in regulating pro-inflammatory cytokines, including IL6 and CCL2(42, 43). In our system, knockdown of TEAD3 or TEAD4 moderately reduced 4mix-induced CCL2, whereas IL6 expression remained largely unchanged, suggesting that inflammatory gene regulation differs among TEAD isoforms.

To compare TEAD- and YAP/TAZ-associated transcriptional programs, we performed RNA-seq in 4mix-treated RASFs following transfection with siTEAD1/3/4 (Fig. 4*C*) or siYAP/TAZ (Fig. 4*D*). As shown in the Venn diagram (Fig. 4*E*), differentially expressed genes partially overlapped between the two perturbations. Canonical targets including ANKRD1, CTGF, and DKK1 were commonly downregulated. In contrast, inflammatory genes including CCL7, IL1R1, and LIF were preferentially suppressed following TEAD knockdown, whereas cell-cycle-associated genes including E2F1, FOXM1, and STMN1 were more prominently reduced following YAP/TAZ knockdown. Consistent with this distinction, phosphorylation of Rb was suppressed following siYAP/TAZ but not siTEAD1/3/4 (Fig. 4*F*), although KEGG pathway analysis demonstrated enrichment of Hippo- and MAPK-related pathways in both conditions (Fig. S3*A*, *B*).

Together, these findings indicate that TEAD isoforms exhibit both redundant and distinct functions in RASFs and regulate transcriptional programs that only partially overlap with those controlled by YAP/TAZ.

Pan-TEAD inhibition suppresses fibroblast pathogenicity and attenuates arthritis without compromising collagen-specific immune responses

Given the functional redundancy among TEAD isoforms (Fig. 4), we next investigated whether pharmacologic inhibition of TEAD activity could suppress pathogenic fibroblast phenotypes using K975, a covalent pan-TEAD inhibitor that targets the palmitate-binding pocket of TEAD proteins and disrupts YAP/TAZ-TEAD-dependent transcription(44). K975 significantly reduced RASF proliferation, as assessed by EdU incorporation, and modestly impaired migratory capacity in scratch assays (Fig. 5*A*, *B*). These findings indicate that pharmacologic TEAD inhibition suppresses key features of fibroblast activation in vitro.

We next evaluated the therapeutic effects of TEAD inhibition in the collagen-induced arthritis (CIA) model. Based on previous studies in mesothelioma(44), we first established an effective dosing regimen for K975. In the preventive setting, oral administration of K975 dose-dependently reduced clinical arthritis severity (Fig. 5*C*). We then evaluated K975 in combination with a suboptimal dose of the TNF inhibitor etanercept (ETN)(45) (Fig. 5*D*). Combination treatment further reduced arthritis severity compared with either monotherapy (Fig. 5*D*). Histological analyses demonstrated reduced synovial inflammation, bone erosion, and cartilage damage, with the greatest improvement observed in the combination

group (Fig. 5*E* and Fig. S4*A*, *B*). Consistent with these findings, fibroblast activation, assessed by fibroblast activation protein (FAP) staining, was also reduced following K975 treatment (Fig. 5*E* and Fig. S4*C*), consistent with reduced fibroblast activation in vivo. In a therapeutic protocol initiated after disease onset, all treatment groups attenuated further disease progression, although reversal of established arthritis was not observed (Fig. 4*D*).

To determine whether TEAD inhibition altered adaptive immune responses, we measured antigen-specific responses in the CIA model. IFN-γ production by splenocytes restimulated ex vivo with type II collagen (CII) was not significantly altered by K975, either alone or in combination with ETN (Fig. 5*F*). Likewise, serum anti-CII IgG1 and IgG2a levels remained unchanged following K975 treatment (Fig. 5*G*), indicating that pharmacologic TEAD inhibition did not substantially affect collagen-specific adaptive immune responses.

Taken together, these findings demonstrate that pan-TEAD inhibition suppresses arthritis progression in the CIA model while preserving collagen-specific adaptive immunity and support TEAD inhibition as a potential fibroblast-directed therapeutic strategy for rheumatoid arthritis.

Discussion

Recent single-cell transcriptomic and spatial analyses of RA synovial tissues have revealed substantial heterogeneity among synovial fibroblasts, with specific subsets contributing to treatment resistance. The pauci-immune pathotype, characterized by fibroblast dominance, has been associated with multidrug-resistant RA(13, 14). Several RASF subsets, including THY1^+DKK3^+, PDPN^+ITGA5^+, and more recently THY1^+COMP^high fibroblasts, have emerged as key populations associated with D2T RA(9, 10). COMP^high fibroblasts, characterized by high expression of cartilage oligomeric matrix protein (COMP), localize to perivascular niches, exhibit persistent TGF-β activation, and persist despite immune cell depletion(10), supporting a fibroblast-intrinsic mechanism of disease persistence. Using nuclear DIA-MS proteomics, we identified TEAD4 as an IFN-γ-responsive transcription factor associated with these pathogenic fibroblast states. In parallel, pharmacologic inhibition of TEAD activity suppressed arthritis in the CIA model. Together, these findings identify TEAD signaling as a candidate regulatory pathway associated with pathogenic fibroblast programs in rheumatoid arthritis.

Our findings identify TEAD4 as an IFN-γ-responsive transcription factor linking inflammatory signaling with TGF-β-associated mechanotransduction in synovial fibroblasts (Fig. 6). TEAD4 activity was enriched in pathogenic fibroblast subsets associated with treatment-resistant RA, suggesting that IFN-γ-dependent induction of TEAD4 may contribute to the maintenance of these disease-relevant fibroblast states. Although crosstalk between IFN-γ and Hippo signaling has not been well characterized, recent studies in cancer have shown that IFN-γ promotes YAP nuclear condensation and enhances TEAD-dependent transcription, thereby contributing to resistance to immune checkpoint inhibitors(46). The increased TEAD4 expression observed in RA synovial tissues compared with OA, in both

lining and sublining fibroblasts (Fig. 2*D*), is consistent with enhanced STAT1 activation described in recent spatial transcriptomic studies(8). While TGF-β-dependent mechanotransduction has been implicated in pathogenic fibroblast subsets, RA is fundamentally an inflammatory disease, raising the question of how inflammatory cytokines are coupled to fibrogenic transcriptional programs. Our findings support a model in which TEAD4 may participate in integrating IFN-γ-mediated inflammatory signaling with TGF-β-associated fibroblast activation. Consistent with this concept, a recent scRNA-seq study identified an ITGA5^+ fibroblast subset activated by both IFN-γ and TGF-β(9). Furthermore, suppression of TEAD4 expression by JAK inhibitors raises the possibility that modulation of TEAD-dependent transcription may contribute to some of the stromal effects of JAK inhibition in RA.

Our data further support a role for TEAD4 in regulating transcriptional programs associated with treatment-resistant fibroblast states. TEAD4 knockdown suppressed multiple genes previously identified in non-responder RA synovial tissues from the R4RA trial, as well as signature genes of the DKK3^+ and THY1^high fibroblast subsets (Fig. 3*C*). Notably, TEAD4 knockdown significantly reduced the expression of COMP and other extracellular matrix-associated genes, including PRELP, which are characteristic markers of the recently described COMP^high fibroblast subset(10, 13). This subset localizes to perivascular regions, exhibits persistent TGF-β pathway activation, and has been associated with non-remission and treatment resistance. Together with our observation that TEAD4 activity is enriched in pathogenic fibroblast subsets, these findings support an association between TEAD4-dependent transcriptional programs and fibroblast states linked to treatment resistance in RA. Further studies using independent D2T RA cohorts will be required to determine the clinical relevance of TEAD4 as a biomarker or therapeutic target in treatment-resistant disease.

While TEAD4 was identified as an IFN-γ-responsive transcription factor, our functional analyses indicate that TEAD-dependent transcriptional regulation is not restricted to TEAD4 alone but involves multiple TEAD family members. Consistent with this, siRNA experiments demonstrated both redundant and isoform-specific functions of TEAD1, TEAD3, and TEAD4 in regulating canonical target genes as well as fibroblast-associated transcriptional programs. These observations provide a rationale for targeting TEAD activity at the family level rather than focusing on a single TEAD isoform. Most currently available TEAD inhibitors disrupt YAP/TAZ-TEAD interactions and therefore share overlapping mechanisms with YAP/TAZ inhibition. Previous studies demonstrated that conditional deletion of YAP1 or pharmacologic inhibition of YAP-TEAD interactions using verteporfin ameliorates experimental arthritis(22). Our comparative analyses likewise identified substantial overlap between TEAD- and YAP/TAZ-regulated transcriptional programs, while also revealing gene sets that were differentially affected by the two perturbations. These findings suggest that TEAD and YAP/TAZ perturbation produce overlapping, but not identical, transcriptional responses in RASFs. The differences observed may reflect the broader interaction network of TEAD proteins. In addition to YAP/TAZ, TEAD proteins interact with other cofactors, including members of the

VGLL family, which can influence transcriptional output. Recent studies further suggest that certain TEAD inhibitors alter the balance between YAP/TAZ and VGLL4 interactions rather than simply blocking TEAD activity(47). Consequently, genetic depletion of TEAD proteins and pharmacologic inhibition of TEAD activity may not be functionally equivalent. Together, our findings support TEAD inhibition as a complementary approach for modulating fibroblast-associated transcriptional programs within the Hippo pathway. Although pan-TEAD inhibitors may be associated with class-specific toxicities, including reversible renal effects(48), the development of isoform-selective inhibitors and TEAD degraders may provide opportunities for more selective therapeutic intervention in fibroblast-driven diseases(49).

This study has several limitations. First, the number of RA and OA synovial tissue samples was limited, and disease duration varied among patients. These factors may have influenced TEAD4 expression and YAP/TAZ-TEAD pathway activity. Second, although our loss-of-function analyses demonstrate that TEAD4 contributes to pathogenic fibroblast transcriptional programs, the sufficiency of TEAD4 to drive these programs was not directly examined. Gain-of-function approaches will therefore be important to further define the role of TEAD4 in regulating pathogenic fibroblast states. Third, the contribution of TEAD4 to disease-relevant fibroblast functions beyond proliferation and migration, including tissue invasion and interactions with other joint-resident cells, remains to be determined. Fourth, the fibroblast-specific contribution of TEAD inhibition to arthritis amelioration was not directly addressed in vivo. Fibroblast-specific genetic models will be required to distinguish cell-intrinsic effects from those mediated by other cell types. Finally, the mechanisms underlying TEAD isoform-specific target gene selection remain incompletely understood. Integrated epigenomic approaches, including ChIP-seq and ATAC-seq, together with proteomic analyses, will help define TEAD-dependent regulatory networks in pathogenic synovial fibroblasts.

In summary, we identify TEAD4 as an IFN-γ-responsive transcription factor associated with pathogenic synovial fibroblast programs in rheumatoid arthritis. Using nuclear proteomics together with transcriptomic and functional analyses, we demonstrate that TEAD4 regulates transcriptional programs linked to treatment-resistant fibroblast states and that pharmacologic TEAD inhibition suppresses fibroblast activation and experimental arthritis without compromising collagen-specific adaptive immunity. Together, these findings identify TEAD signaling as a therapeutically targetable pathway in rheumatoid arthritis and provide a framework for understanding how inflammatory and profibrotic signaling converge in pathogenic synovial fibroblasts.

Methods

Study approval. The study protocol involving human participants was approved by the Ethics Committee of the Institute of Science Tokyo (Approval Nos. M2000-979 and G2018-028). Written informed consent was obtained from all participants prior to sample collection. All animal experiments were approved by the

Experimental Animal Ethics Committee of the Institute of Science Tokyo (Approval No. A2025034C2).

Patient recruitment and synovial fibroblast isolation. Synovial tissues were obtained from eight patients with RA and three patients with OA undergoing arthroplasty after written informed consent. Clinical characteristics are summarized in Table S1. Synovial tissues were enzymatically digested with collagenase type IV, dispase II, and DNase I, followed by erythrocyte lysis. Isolated RASFs were cultured in Dulbecco's modified Eagle's medium (DMEM) supplemented with 10% fetal bovine serum (FBS), penicillin, and streptomycin and were used between passages 5 and 10.

DIA-MS sample preparation. RASFs (n = 3) were stimulated with TNF-α (1 ng/mL), IL-1β (0.1 ng/mL), IFN-γ (10 ng/mL), and TGF-β1 (1 ng/mL) (4mix) for 24 h. Nuclear and cytoplasmic fractions were prepared using the PIPER Nuclear Protein Extraction Kit (Invitrogen). Nuclear proteins were solubilized in 100 mM Tris-HCl (pH 8.0) containing 4% sodium dodecyl sulfate and 20 mM NaCl using a BIORUPTOR BR-II (SONICBIO Co., Kanagawa, Japan). Protein extracts were reduced with 20 mM tris(2-carboxyethyl)phosphine at 80°C for 10 min and alkylated with 30 mM iodoacetamide at room temperature for 30 min in the dark. Protein purification and digestion were performed using the SP3 method. Proteins were digested overnight at 37°C using Trypsin/Lys-C Mix (Promega) at 500 ng/μL. Digested peptides were purified using GL-Tip SDB (GL Sciences), dissolved in 2% acetonitrile containing 0.1% trifluoroacetic acid, and quantified using a bicinchoninic acid (BCA) assay to a final concentration of 200 ng/μL.

LC-MS/MS and data processing. Digested peptides (500 ng) were separated on a 75 μm × 12 cm nanoLC capillary column (Nikkyo Technos, Tokyo, Japan) maintained at 60°C using an UltiMate 3000 RSLCnano LC system (Thermo Fisher Scientific). Peptides were eluted over a 100-min gradient using mobile phase A (0.1% formic acid in water) and mobile phase B (0.1% formic acid in 80% acetonitrile) at a flow rate of 150 nL/min. The gradient was programmed as follows: 7% B at 0 min, 37% B at 88 min, and 70% B at 94–100 min. Eluting peptides were analyzed using a quadrupole Orbitrap Exploris 480 hybrid mass spectrometer (Thermo Fisher Scientific) operated in data-independent acquisition (DIA) mode. MS1 spectra were acquired over an m/z range of 490–745 at a resolution of 15,000 with an automatic gain control (AGC) target of 3 × 10^6. MS2 spectra were acquired over an m/z range of 200–1,800 at a resolution of 45,000 using a fixed normalized collision energy of 26%, an AGC target of 3 × 10^6, and an isolation width of 4 m/z. Data were processed in Scaffold DIA (Proteome Software Inc.) using an optimized acquisition window scheme for the m/z 500–740 range. Raw DIA data were searched against an in silico–predicted spectral library generated by DIA-NN (version 1.8.1) from the UniProt human reference proteome (UP000005640, reviewed canonical sequences; 20,588 entries).

Western blotting. Cells were lysed in 2% SDS sample buffer containing Complete Mini Protease Inhibitor (Roche) and Phosphatase Inhibitor Cocktail (Sigma-Aldrich), followed by SDS-PAGE and immunoblotting. Primary antibodies included pan-TEAD (Cell Signaling Technology, #13295, 1:1,000), TEAD4 (Abcam,

ab58310, 1:1,000), YAP/TAZ (Cell Signaling Technology, #8418, 1:1,000; Santa Cruz Biotechnology, sc-101199, 1:200), Lamin A/C (Active Motif, #39287, 1:1,000), GAPDH (Cell Signaling Technology, #97166, 1:1,000), phospho-Rb (Ser807/811; Cell Signaling Technology, #9308, 1:1,000), Rb (Cell Signaling Technology, #9302, 1:1,000), and β-actin (Sigma-Aldrich, A2228, 1:5,000). Immunoreactive bands were visualized using ECL Prime Western Blotting Detection Reagent (Amersham) and imaged with an ImageQuant LAS-4000 system (Fujifilm).

Quantitative real-time PCR. Total RNA was extracted, reverse transcribed, and analyzed by quantitative real-time PCR (qPCR) using a LightCycler 96 system (Roche) with SYBR Green PCR Master Mix (Qiagen). Relative gene expression was calculated using the ΔΔCt method with GAPDH as the internal reference. Primer sequences are listed in Table S2.

Immunohistochemistry. For histological analyses, synovial tissues from patients with RA or OA and hind paws from CIA mice were fixed in 10% neutral-buffered formalin. Hind paws were decalcified in 0.5 M EDTA before paraffin embedding. Tissue sections were stained with antibodies against fibroblast activation protein (FAP; Abcam, ab207178, 1:100). Immunoreactivity was visualized using DAB substrate, and images were acquired using a BX-50 microscope (Olympus Optical, Tokyo, Japan).

siRNA knockdown. RASFs were transfected with Silencer Select siRNAs targeting TEAD1 (S13961), TEAD3 (S13967), TEAD4 (S13964 and S13966), YAP1 (S20366), WWTR1 (TAZ) (S24787), or Silencer Select Negative Control No. 2 (Thermo Fisher Scientific) using Lipofectamine RNAiMAX (Thermo Fisher Scientific). After 72 h, cells were stimulated with TNF-α (1 ng/mL), IL-1β (0.1 ng/mL), IFN-γ (10 ng/mL), and TGF-β1 (1 ng/mL) (4mix) for an additional 24 h.

RNA sequencing. RNA sequencing was performed using RASFs transfected with control or target-specific siRNAs and subsequently stimulated with 4mix. Library preparation and sequencing were performed by BGI (Hong Kong, China) using the DNBSEQ platform. Total RNA (RNA integrity number ≥7) was subjected to poly(A) enrichment or rRNA depletion, followed by fragmentation and reverse transcription. Strand-specific cDNA libraries were constructed, adaptor ligated, PCR amplified, circularized into DNA nanoballs, and sequenced as 100-bp paired-end reads. Differentially expressed genes (DEGs) were identified using DESeq2 (adjusted $q \leq 0.05$). KEGG pathway enrichment analysis and wPGSA(27) were performed to evaluate pathway activity and transcription factor regulation.

wPGSA analysis of scRNA-seq data. Published human RASF scRNA-seq data were reanalyzed using wPGSA. The original dataset had been preprocessed by the authors, including sample integration, dimensionality reduction, clustering, and cell-type annotation(7). The dataset comprised RASFs isolated from patients with active RA or RA in remission and identified five transcriptionally distinct fibroblast subsets. To infer transcription factor activity in active relative to remission-state RASFs, $\log_2$ fold changes were calculated using the FindMarkers function in Seurat and used as input for wPGSA. Transcription factors with an adjusted q value <0.05 were considered significantly altered. In addition, transcription factor

activity scores were calculated from normalized gene expression values within each fibroblast subset to compare predicted transcription factor activities between active and remission samples.

EdU incorporation assay. RASFs were incubated with 1 μM 5-ethynyl-2′-deoxyuridine (EdU) for 24 h and analyzed using the Click-iT EdU Flow Cytometry Cell Proliferation Kit (Thermo Fisher Scientific) according to the manufacturer's instructions. After labeling with Alexa Fluor 655, cells were analyzed on a FACSLyric flow cytometer (BD Biosciences), and data were processed using FlowJo software.

Cell migration assay. RASFs were cultured in DMEM supplemented with 10% FBS until reaching 80–90% confluence. A linear scratch (~1 mm wide) was introduced using a sterile pipette tip, and cells were cultured for an additional 24 h. Wound closure was monitored microscopically. Images were acquired using a BioZero microscope (Keyence, Osaka, Japan) and quantified using ImageJ software.

Collagen-induced arthritis model. Collagen-induced arthritis (CIA) was induced in six-week-old male DBA/1J mice using bovine type II collagen (CII) emulsified in complete Freund's adjuvant (CFA; Chondrex) as previously described(45). Mice were immunized by intradermal injection at the base of the tail on day 0, followed by a booster immunization with CII emulsified in incomplete Freund's adjuvant (IFA; Chondrex) on day 21. Arthritis severity was evaluated using a clinical score ranging from 0 to 4 for each limb (maximum score of 16): 0, no swelling; 1, mild swelling involving one joint; 2, moderate swelling involving multiple joints; 3, severe swelling involving two or more joints; and 4, severe swelling with ankylosis involving multiple joints. Histological scoring of synovial inflammation, bone erosion, and cartilage damage was performed as previously described(50).

Treatment protocol. K975 (Accela) was suspended in 0.5% methylcellulose 400 and administered orally twice daily at doses of 100 or 300 mg/kg. Etanercept (ETN; 3 mg/kg) was administered intraperitoneally every 3 days either from days 21–35 (preventive protocol) or days 31–42 (therapeutic protocol), as previously described(44, 45).

Splenocyte restimulation assay. Splenocytes were harvested on day 35 and cultured with heat-denatured bovine type II collagen (30 μg/mL) for 3 days. IFN-γ concentrations in culture supernatants were quantified using a mouse IFN-γ ELISA kit (R&D Systems).

Anti-type II collagen IgG ELISA. Serum samples were collected on day 35. Anti-CII IgG1 and IgG2a antibody titers were measured by ELISA as previously described(51). ELISA plates were coated with heat-denatured bovine type II collagen (1 μg/mL), incubated with serially diluted serum samples, and detected using HRP-conjugated anti-mouse IgG1 (ZYMED, 61-0120) or IgG2a (Invitrogen, 61-0320) antibodies. Signals were developed using TMB substrate and quantified by absorbance measurement.

Statistical analysis. Data are presented as mean ± SD or SEM, as indicated in the figure legends. Comparisons between two groups were performed using two-sided Student's *t* test or the two-sided Wilcoxon signed-rank test, as appropriate.

Multiple-group comparisons were performed using one-way ANOVA followed by Dunnett's multiple-comparison test or two-way ANOVA, as indicated. A two-sided *P* value <0.05 was considered statistically significant. Statistical analyses were performed using the limma package in R and GraphPad Prism 9 (GraphPad Software).

Data availability

The datasets generated and analyzed during the current study are available from the corresponding author upon reasonable request. The RNA-seq data used in the current study are available at NCBI GEO under accession number GSE305532, GSE306632, GSE 328455, and GSE328455.

Acknowledgments

This work was supported by Japan Agency for Medical Research and Development (AMED) under grant number 21ek0410061h0003 and 25ek0410134h0001 and JSPS KAKENHI under grant number 22K08519 and 21K16301.

References

1. E. M. Gravallese, G. S. Firestein, Rheumatoid Arthritis — Common Origins, Divergent Mechanisms. *N. Engl. J. Med.* **388**, 529–542 (2023).
2. J. S. Smolen, D. Aletaha, I. B. McInnes, Rheumatoid arthritis. *Lancet* **388**, 2023–2038 (2016).
3. A. E. Zou, S. Kongthong, A. A. Mueller, M. B. Brenner, Fibroblasts in immune responses, inflammatory diseases and therapeutic implications. *Nat. Rev. Rheumatol.* **21**, 336–354 (2025).
4. G. Nagy, *et al.*, EULAR definition of difficult-To-Treat rheumatoid arthritis. *Ann. Rheum. Dis.* **80**, 31–35 (2021).
5. F. Mizoguchi, *et al.*, Functionally distinct disease-associated fibroblast subsets in rheumatoid arthritis. *Nat. Commun.* **9**, 1–11 (2018).
6. F. Zhang, *et al.*, Defining inflammatory cell states in rheumatoid arthritis joint synovial tissues by integrating single-cell transcriptomics and mass cytometry. *Nat. Immunol.* **20**, 928–942 (2019).
7. S. Alivernini, *et al.*, Distinct synovial tissue macrophage subsets regulate inflammation and remission in rheumatoid arthritis. *Nat. Med.* **26**, 1295–1306 (2020).
8. M. H. Smith, *et al.*, Drivers of heterogeneity in synovial fibroblasts in rheumatoid arthritis. *Nat. Immunol.* **24**, 1200–1210 (2023).
9. L. Zheng, *et al.*, ITGA5+ synovial fibroblasts orchestrate proinflammatory niche formation by remodelling the local immune microenvironment in rheumatoid arthritis. *Ann. Rheum. Dis.* **84**, 232–252 (2025).
10. K. Bhamidipati, *et al.*, Spatial patterning of fibroblast TGFβ signaling underlies treatment resistance in rheumatoid arthritis. *Nat. Immunol.* **27** (2026).
11. K. Wei, *et al.*, Notch signalling drives synovial fibroblast identity and arthritis pathology. *Nature* **582**, 259–264 (2020).

12. A. A. Mueller, *et al.*, Wnt signaling drives stromal inflammation in inflammatory arthritis. *bioRxiv* (2025).
13. F. Rivellese, *et al.*, Rituximab versus tocilizumab in rheumatoid arthritis: synovial biopsy-based biomarker analysis of the phase 4 R4RA randomized trial. *Nat. Med.* **28**, 1256–1268 (2022).
14. F. Zhang, *et al.*, Deconstruction of rheumatoid arthritis synovium defines inflammatory subtypes. *Nature* **623**, 616–624 (2023).
15. A. P. Croft, *et al.*, Distinct fibroblast subsets drive inflammation and damage in arthritis. *Nature* **570**, 246–251 (2019).
16. A. G. Pratt, *et al.*, Targeting synovial fibroblast proliferation in rheumatoid arthritis (TRAFIC): an open-label, dose-finding, phase 1b trial. *Lancet Rheumatol.* **3**, e337–e346 (2021).
17. D. Tasaki, *et al.*, A double-blind, placebo-controlled, randomized multiple dose phase 1b trial of a CDK4/6 inhibitor, TCK-276, in patients with active rheumatoid arthritis. *Rheumatology* **64**, 1036–1044 (2025).
18. T. Hosoya, T. Saito, S. Yasuda, Cyclin dependent kinase inhibitor: A long-Awaited, late-coming, novel class agent in rheumatoid arthritis. *Rheumatology* **64**, 916–918 (2025).
19. M. Fu, *et al.*, The Hippo signalling pathway and its implications in human health and diseases. *Signal Transduct. Target. Ther.* **7** (2022).
20. A. Totaro, T. Panciera, S. Piccolo, YAP/TAZ upstream signals and downstream responses. *Nat. Cell Biol.* **20**, 888–899 (2018).
21. X. He, *et al.*, Myofibroblast YAP/TAZ activation is a key step in organ fibrogenesis. *JCI Insight* **7** (2022).
22. R. A. Symons, *et al.*, Targeting the IL-6–Yap–Snail signalling axis in synovial fibroblasts ameliorates inflammatory arthritis. *Ann. Rheum. Dis.* **81**, 214–224 (2022).
23. R. Caire, *et al.*, YAP/TAZ: Key Players for Rheumatoid Arthritis Severity by Driving Fibroblast Like Synoviocytes Phenotype and Fibro-Inflammatory Response. *Front. Immunol.* **12**, 1–16 (2021).
24. A. Bottini, *et al.*, PTPN14 phosphatase and YAP promote TGFβ signalling in rheumatoid synoviocytes. *Ann. Rheum. Dis.* **78**, 600–609 (2019).
25. Y. Tagawa, *et al.*, ARID5B is a negative modulator of IL-6 production in rheumatoid arthritis synovial fibroblasts. *Immunol. Med.* **47**, 176–185 (2024).
26. M. Sato, *et al.*, Reciprocal Regulation of GLI1 and GLI3 Fine Tunes the Pathogenic Behavior of Synovial Fibroblasts in Rheumatoid Arthritis. *Int. J. Rheum. Dis.* **29**, 1–12 (2026).
27. E. Kawakami, S. Nakaoka, T. Ohta, H. Kitano, Weighted enrichment method for prediction of transcription regulators from transcriptome and global chromatin immunoprecipitation data. *Nucleic Acids Res.* **44**, 5010–5021 (2016).
28. D. Hecker, *et al.*, Computational tools for inferring transcription factor activity. *Proteomics* **23**, 1–20 (2023).

29. K. Fröhlich, *et al.*, Data-Independent Acquisition: A Milestone and Prospect in Clinical Mass Spectrometry–Based Proteomics. *Mol. Cell. Proteomics* **23**, 100800 (2024).
30. A. J. Federation, *et al.*, Highly Parallel Quantification and Compartment Localization of Transcription Factors and Nuclear Proteins. *Cell Rep.* **30**, 2463-2471.e5 (2020).
31. A. Floudas, *et al.*, Distinct stromal and immune cell interactions shape the pathogenesis of rheumatoid and psoriatic arthritis. *Ann. Rheum. Dis.* **81**, 1224–1242 (2022).
32. R. I. Ainsworth, *et al.*, Systems-biology analysis of rheumatoid arthritis fibroblast-like synoviocytes implicates cell line-specific transcription factor function. *Nat. Commun.* **13**, 1–11 (2022).
33. H. Tsuchiya, *et al.*, Parsing multiomics landscape of activated synovial fibroblasts highlights drug targets linked to genetic risk of rheumatoid arthritis. *Ann. Rheum. Dis.* **80**, 440–450 (2021).
34. M. Armaka, *et al.*, Single-cell multimodal analysis identifies common regulatory programs in synovial fibroblasts of rheumatoid arthritis patients and modeled TNF-driven arthritis. *Genome Med.* **14**, 1–25 (2022).
35. M. Yan, *et al.*, programs in disease-associated fibroblasts. **23** (2022).
36. A. Pelissier, T. Laragione, C. Harris, M. Rodríguez Martínez, P. S. Gulko, BACH1 as a key driver in rheumatoid arthritis fibroblast-like synoviocytes identified through gene network analysis. *Life Sci. Alliance* **8**, 1–15 (2025).
37. A. V. Pobbati, R. Kumar, B. P. Rubin, W. Hong, Therapeutic targeting of TEAD transcription factors in cancer. *Trends Biochem. Sci.* **48**, 450–462 (2023).
38. F. Zanconato, *et al.*, Genome-wide association between YAP/TAZ/TEAD and AP-1 at enhancers drives oncogenic growth. *Nat. Cell Biol.* **17**, 1218–1227 (2015).
39. Z. Zou, T. Ohta, S. Oki, ChIP-Atlas 3.0: A data-mining suite to explore chromosome architecture together with large-scale regulome data. *Nucleic Acids Res.* **52**, W45–W53 (2024).
40. P. G. Traves, *et al.*, JAK selectivity and the implications for clinical inhibition of pharmacodynamic cytokine signalling by filgotinib, upadacitinib, tofacitinib and baricitinib. *Ann. Rheum. Dis.* **80**, 865–875 (2021).
41. M. H. Schiff, Role of interleukin 1 and interleukin 1 receptor antagonist in the mediation of rheumatoid arthritis. *Ann. Rheum. Dis.* **59**, 103–108 (2000).
42. X. Guo, *et al.*, Single tumor-initiating cells evade immune clearance by recruiting type II macrophages. *Genes Dev.* **31**, 247–259 (2017).
43. L. He, *et al.*, Yap and taz are transcriptional co-activators of ap-1 proteins and stat3 during breast cellular transformation. *Elife* **10**, 1–26 (2021).
44. A. Kaneda, *et al.*, The novel potent TEAD inhibitor, K-975, inhibits YAP1/TAZ-TEAD protein-protein interactions and exerts an anti-tumor

effect on malignant pleural mesothelioma. *Am. J. Cancer Res.* **10**, 4399–4415 (2020).
45. T. Hosoya, *et al.*, Cell cycle regulation therapy combined with cytokine blockade enhances antiarthritic effects without increasing immune suppression. *Ann. Rheum. Dis.* **75**, 253–259 (2016).
46. M. Yu, *et al.*, Interferon-γ induces tumor resistance to anti-PD-1 immunotherapy by promoting YAP phase separation. *Mol. Cell* **81**, 1216-1230.e9 (2021).
47. A. D. Guarnacciaa, *et al.*, TEAD-targeting small molecules induce a cofactor switch to regulate the Hippo pathway. *Proc. Natl. Acad. Sci.* **122** (2025).
48. S. Paul, J. Sims, T. Pham, A. Dey, Targeting the Hippo pathway in cancer: kidney toxicity as a class effect of TEAD inhibitors? *Trends in Cancer* **11**, 25–36 (2025).
49. H. Chen, *et al.*, Targeted degradation of specific TEAD paralogs by small molecule degraders. *Heliyon* **10**, e37829 (2024).
50. S. Hayer, *et al.*, SMASH recommendations for standardised microscopic arthritis scoring of histological sections from inflammatory arthritis animal models. *Ann. Rheum. Dis.* **80**, 714–726 (2021).
51. T. Saito, *et al.*, Small Molecule Potentiator of Adjuvant Activity Enhancing Survival to Influenza Viral Challenge. *Front. Immunol.* **12**, 1–11 (2021).

Figures and Tables

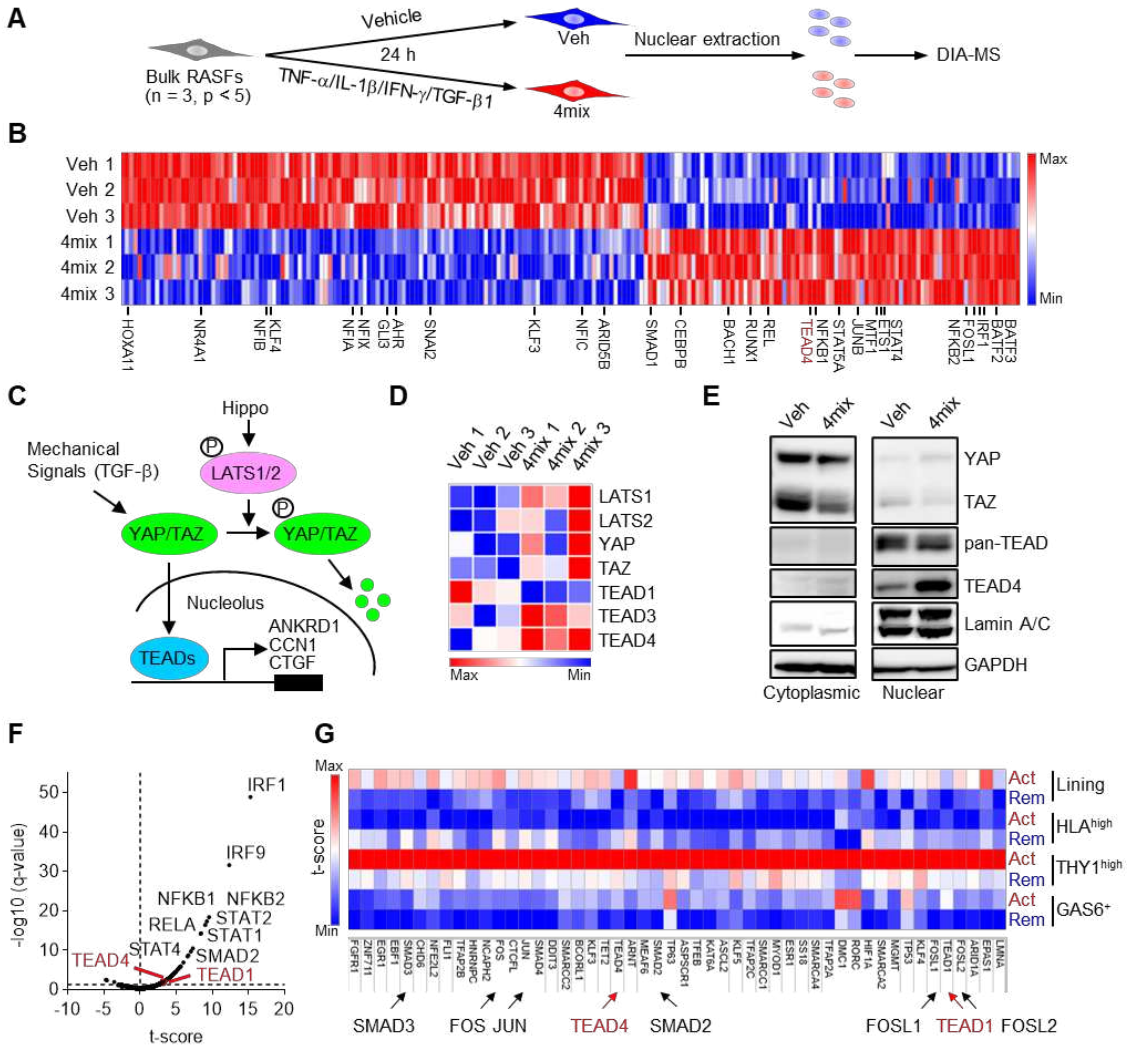


Figure 1. Nuclear proteomics identifies TEAD4 as an IFN-γ-responsive transcription factor enriched in pathogenic RASF subsets. (A) Experimental design. RASFs (n = 3, passages 5–10) were treated with vehicle (DMSO) or a cytokine combination (4mix) consisting of TNF-α (1 ng/mL), IL-1β (0.1 ng/mL), IFN-γ (10 ng/mL), and TGF-β1 (1 ng/mL) for 24 h. Nuclear extracts were analyzed by data-independent acquisition mass spectrometry (DIA-MS). (B) Heatmap showing transcription factors differentially expressed in nuclear extracts from 4mix-treated RASFs compared with vehicle controls ($|\log_2 FC| > 0.65$, $P < 0.05$). (C) Schematic of Hippo signaling and TGF-β-associated mechanotransduction pathways. (D) Heatmap of YAP/TAZ/TEAD pathway-related proteins identified by DIA-MS. (E) Immunoblot analysis of YAP, TAZ, and TEAD proteins in nuclear and cytoplasmic fractions. Lamin A/C and GAPDH served as nuclear and cytoplasmic fraction controls, respectively. (F) wPGSA of RNA-seq data from RASFs treated with vehicle or 4mix for 24 h. Transcription factors identified by both DIA-MS and wPGSA are highlighted (n = 3, $q < 0.05$). (G) Heatmap showing transcription factor activity scores estimated by wPGSA using published scRNA-seq data from RASF subsets. The top 50 transcription factors differentially activated between active and remission samples in the THY1^high subset are shown ($q < 0.05$).

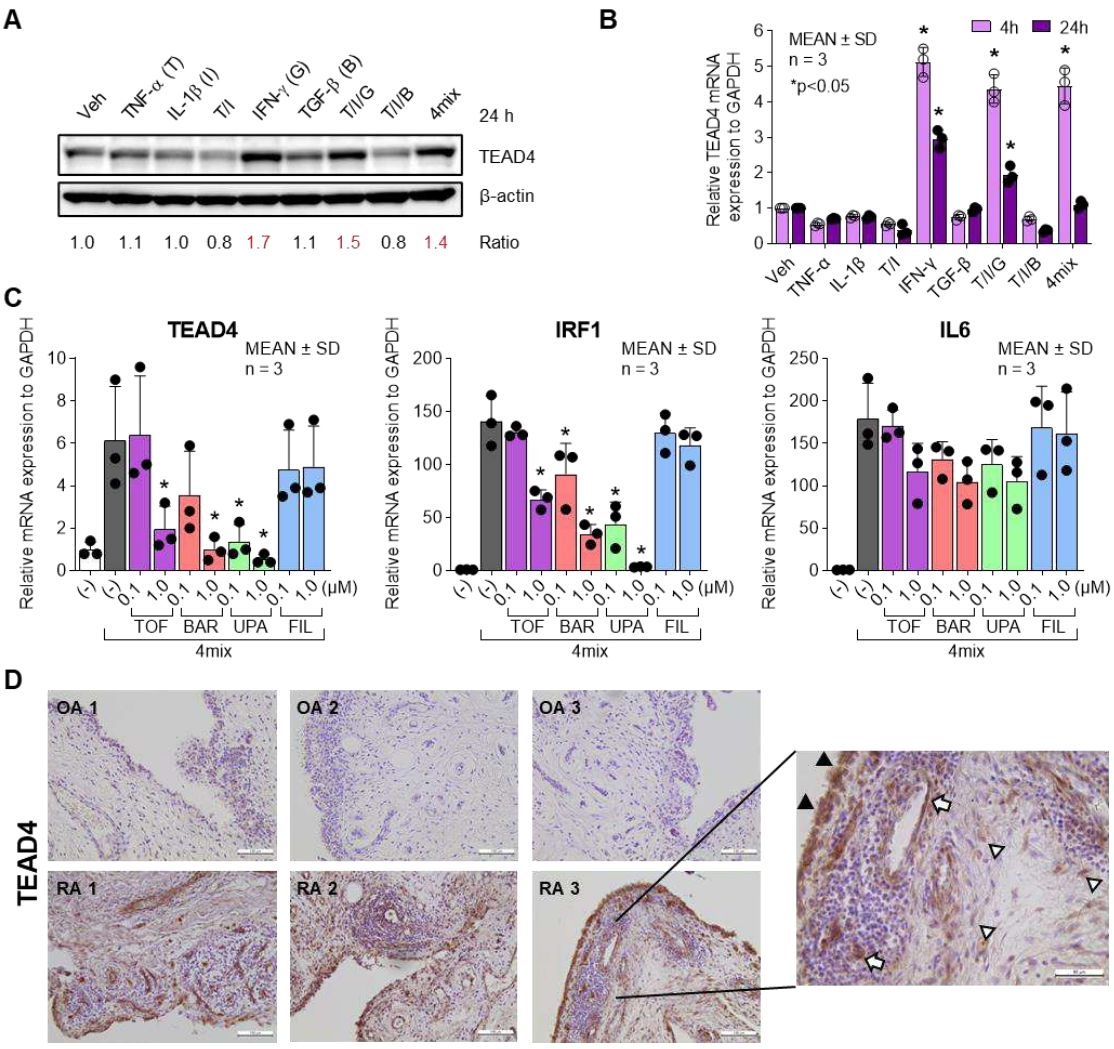


Figure 2. TEAD4 is induced by IFN-γ through the JAK/STAT pathway in rheumatoid arthritis synovial fibroblasts. (A) Immunoblot analysis of TEAD4 protein in RASFs treated with TNF-α, IL-1β, IFN-γ, TGF-β1, or the indicated cytokine combinations for 24 h. Band intensities were normalized to β-actin. (B) qPCR analysis of TEAD4 mRNA expression 4 and 24 h after cytokine stimulation. (C) Effects of JAK inhibitors, including tofacitinib (TOF), baricitinib (BAR), upadacitinib (UPA), and filgotinib (FIL), on TEAD4 expression in 4mix-treated RASFs. (D) Immunohistochemical staining of TEAD4 in synovial tissues from patients with RA and OA. Scale bars, 100 μm. Black arrowheads indicate lining fibroblasts; white arrowheads indicate sublining fibroblasts; white arrows indicate endothelial or mural cells. Data are presented as mean ± SD (n = 3). Statistical significance was determined by one-way ANOVA followed by Dunnett's multiple-comparison test. $P < 0.05$.

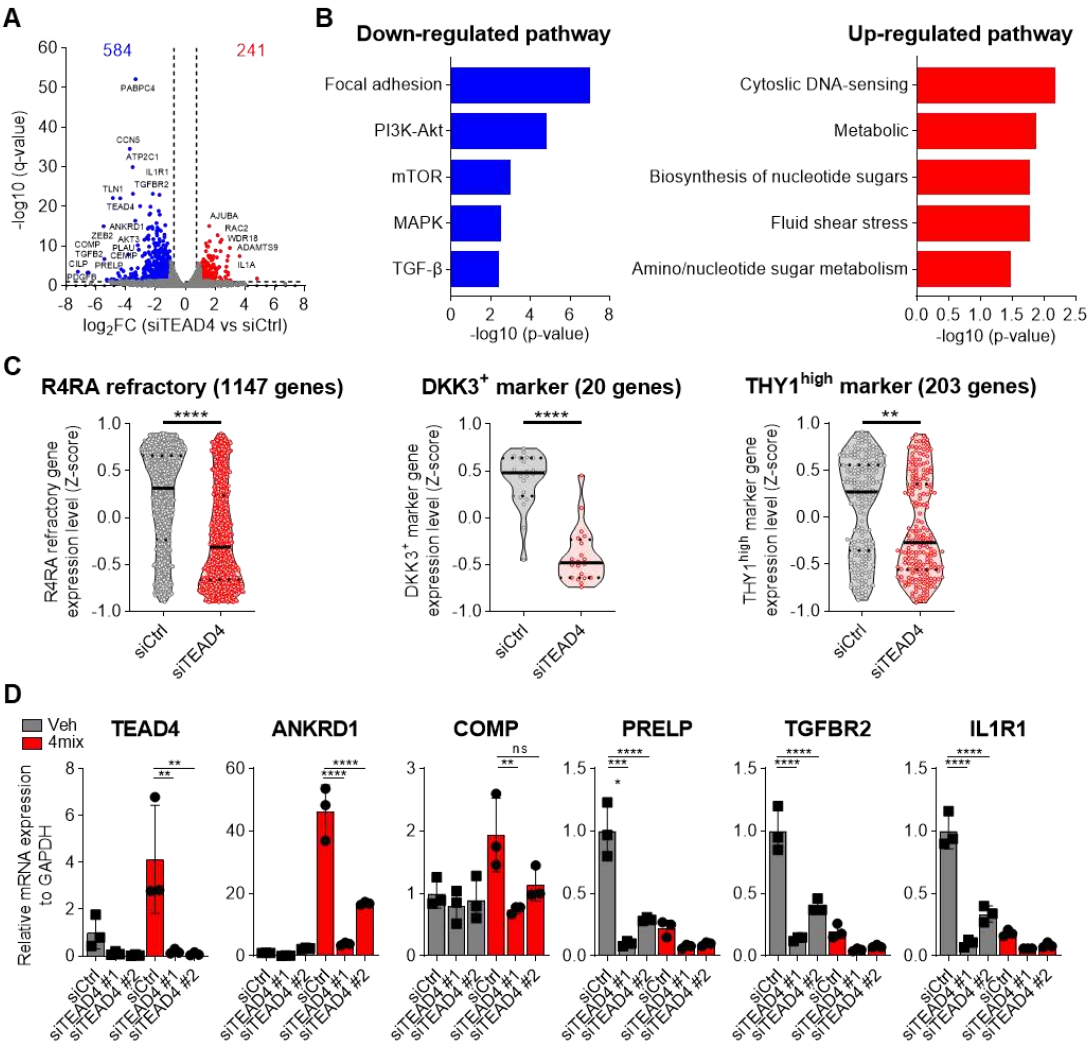


Figure 3. TEAD4 regulates transcriptional programs associated with pathogenic synovial fibroblast subsets. (A) Volcano plot showing differentially expressed genes (DEGs) in 4mix-treated RASFs transfected with control siRNA (siCtrl) or siTEAD4 ($|\log_2 FC| > 1.0$, $q < 0.05$; n = 3). (B) KEGG pathway enrichment analysis of DEGs following TEAD4 knockdown. The top five enriched pathways are shown ($P < 0.05$). (C) Expression of gene signatures associated with treatment-resistant RA and pathogenic fibroblast subsets following TEAD4 knockdown. (D) qPCR validation of selected YAP/TAZ/TEAD target genes and fibroblast-associated genes using two independent siRNAs targeting TEAD4. Data are presented as mean ± SD (n = 3). Statistical significance was determined by two-sided Wilcoxon signed-rank test (C) or one-way ANOVA followed by Dunnett's multiple-comparison test (D). $P < 0.01$, $P < 0.001$, $P < 0.0001$; ns, not significant.

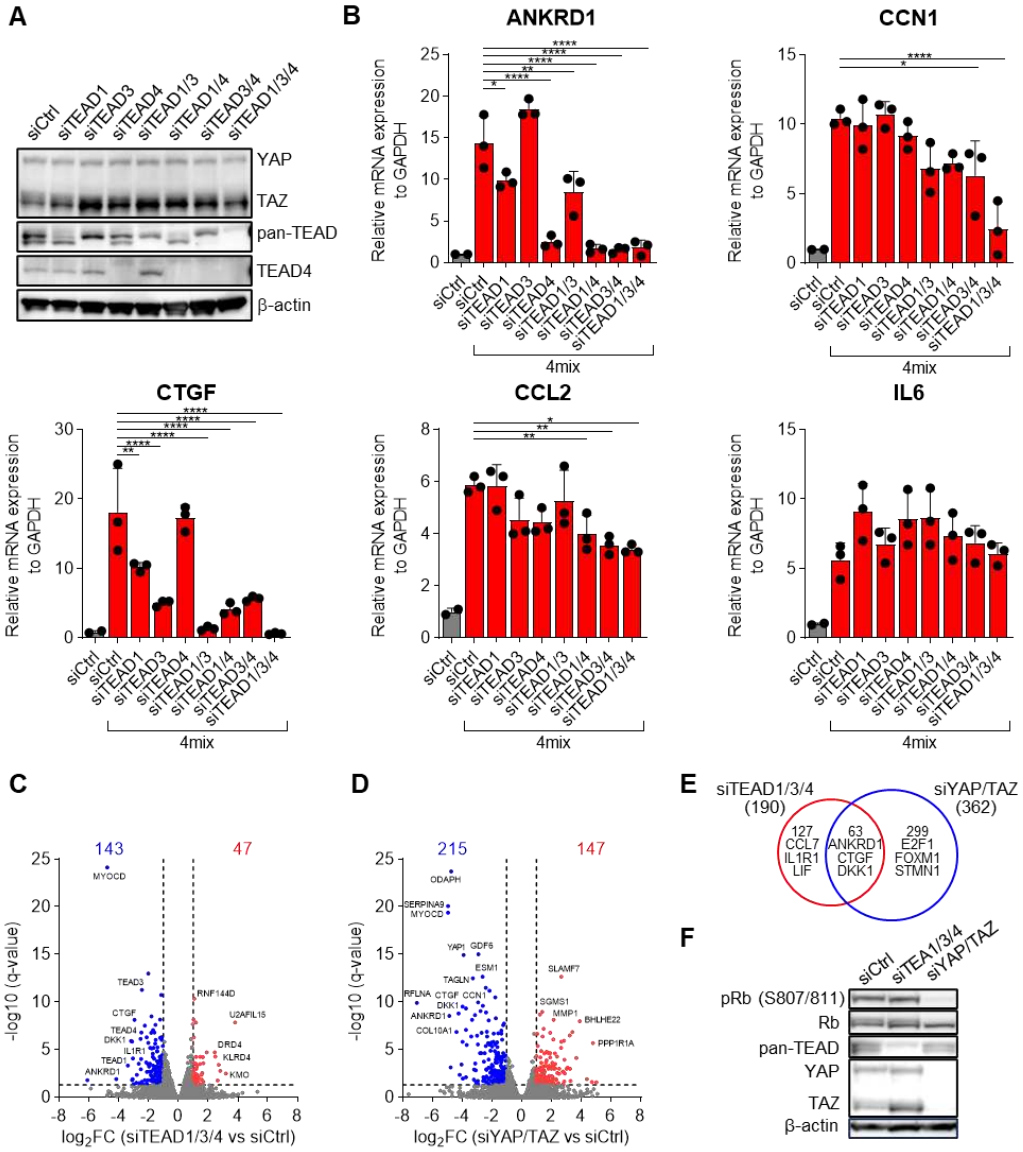


Figure 4. TEAD isoforms exhibit redundant and distinct functions in regulating transcriptional programs in rheumatoid arthritis synovial fibroblasts. (A) Immunoblot analysis of TEAD isoforms in RASFs transfected with individual or combinatorial TEAD siRNAs. (B) qPCR analysis of canonical YAP/TAZ/TEAD target genes in RASFs transfected with the indicated TEAD siRNAs followed by 4mix stimulation. Data are presented as mean ± SD (n = 3). (C, D) Volcano plots showing differentially expressed genes (DEGs) in RASFs transfected with siTEAD1/3/4 (C) or siYAP/TAZ (D) compared with control siRNA (siCtrl) ($|\log_2 FC| > 1.0$, $q < 0.05$; n = 3). (E) Overlap of DEGs identified following TEAD1/3/4 or YAP/TAZ knockdown. (F) Immunoblot analysis of phospho-Rb (Ser807/811) following TEAD1/3/4 or YAP/TAZ knockdown. Statistical significance in (B) was determined by one-way ANOVA followed by Dunnett's multiple-comparison test. $P < 0.05$, $P < 0.01$, $P < 0.0001$.

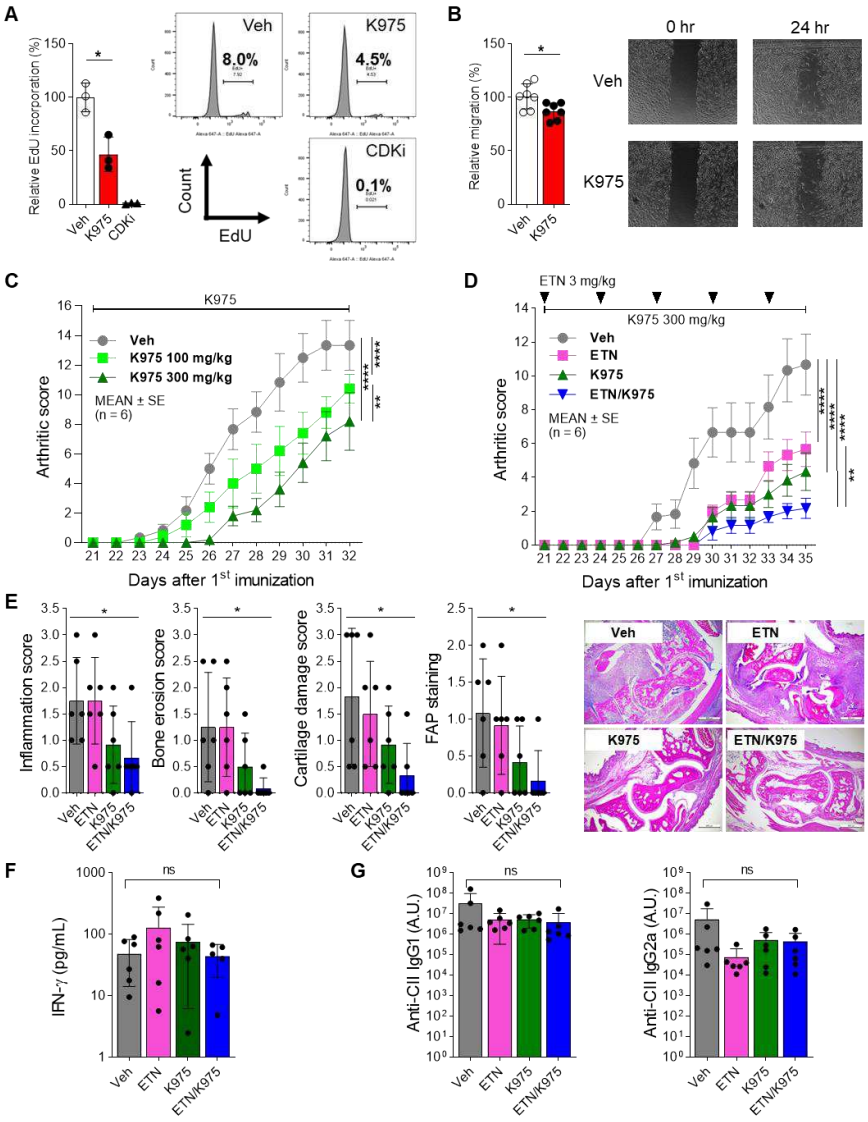


Figure 5. Pan-TEAD inhibition suppresses fibroblast pathogenicity and attenuates arthritis without compromising collagen-specific immune responses. (A) EdU incorporation assay showing reduced proliferation of RASFs following treatment with K975 (0.5 μM). A CDK inhibitor (CDKi) was included as a positive control. (B) Scratch wound-healing assay showing reduced migratory capacity of RASFs following K975 treatment. Representative images and quantitative analysis are shown. (C) Preventive collagen-induced arthritis (CIA) model demonstrating dose-dependent effects of K975 (100 or 300 mg/kg, twice daily) on clinical arthritis scores. (D) Effects of K975 (300 mg/kg) in combination with etanercept (ETN; 3 mg/kg, intraperitoneally administered on days 21, 24, 27, 30, and 33) in the preventive CIA model. (E) Histological evaluation of synovial inflammation, bone erosion, and cartilage damage with representative hematoxylin and eosin (H&E) staining. (F) IFN-γ production by splenocytes following ex vivo restimulation with type II collagen (CII). (G) Serum anti-CII IgG1 and IgG2a antibody levels measured on day 35. Data are presented as mean ± SD (A, B) or mean ± SEM (C–G). Statistical significance was determined by Mann–Whitney *U* test (A, B), one-way ANOVA (F, G), or two-way ANOVA (C, D), as indicated. $P < 0.05$, $P < 0.01$, $P < 0.0001$; ns, not significant.

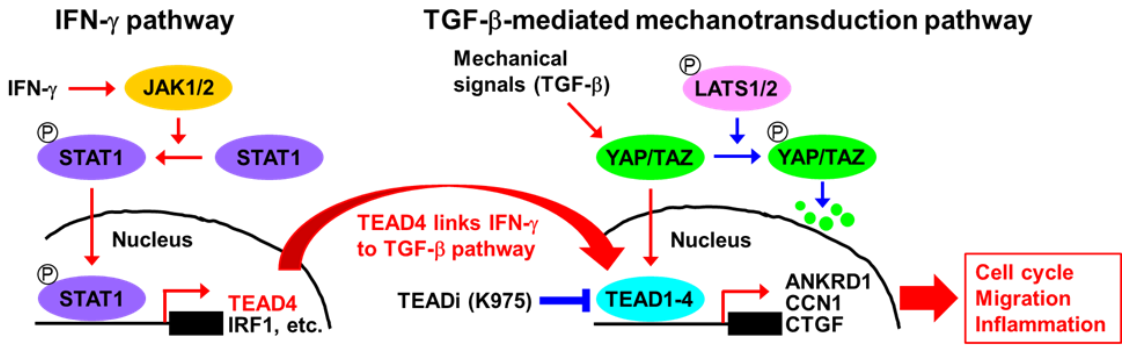


Figure 6. Proposed model of TEAD-dependent regulation of pathogenic fibroblast programs in rheumatoid arthritis. IFN-γ induces TEAD4 expression through the JAK/STAT pathway in synovial fibroblasts. Together with other TEAD family members, TEAD4 contributes to transcriptional programs associated with TGF-β-related mechanotransduction and fibroblast activation. These programs include genes involved in extracellular matrix remodeling, proliferation, inflammation, and treatment-resistant fibroblast states. Pharmacologic inhibition of TEAD suppresses fibroblast activation and attenuates experimental arthritis while preserving collagen-specific adaptive immune responses, supporting TEAD signaling as a potential therapeutic target in rheumatoid arthritis.

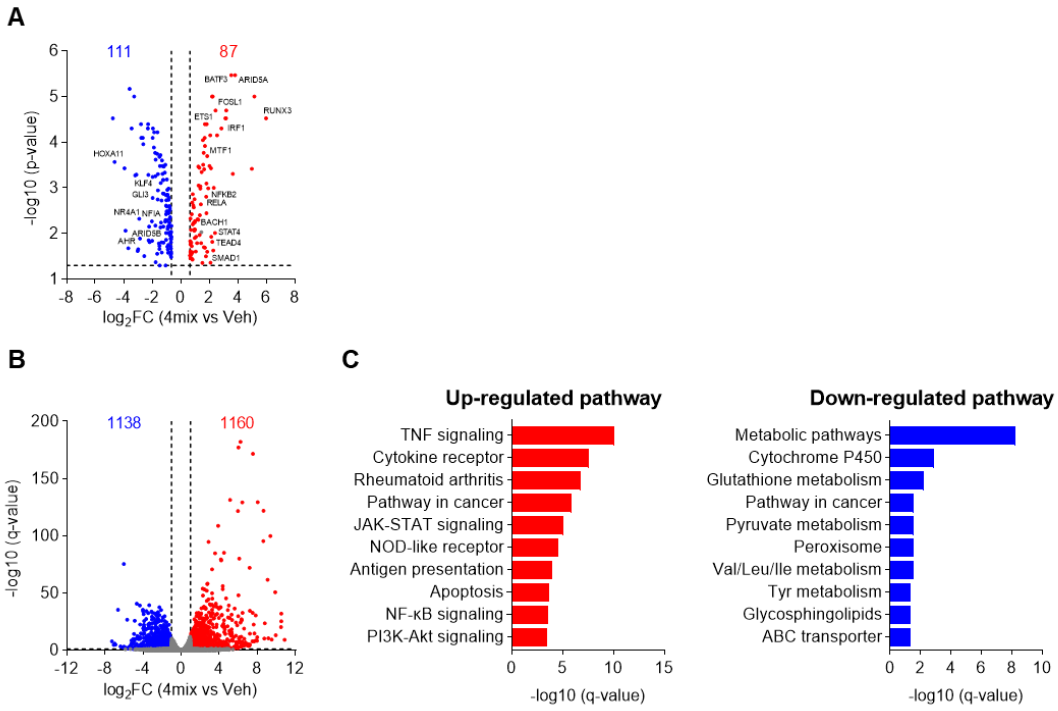


Figure S1. DIA-MS and RNA-seq analyses of RASFs following 4mix stimulation. (A) Volcano plot showing transcription factors differentially expressed in nuclear extracts of RASFs treated with 4mix (TNF-α, IL-1β, IFN-γ, and TGF-β1) compared with vehicle ($|\log_2 FC| > 0.65$, $P < 0.05$; n = 3). (B) Volcano plot showing differentially expressed genes (DEGs) in RASFs following 4mix stimulation compared with vehicle ($|\log_2 FC| > 1.0$, $q < 0.05$; n = 3). (C) KEGG pathway enrichment analysis of DEGs. The top 10 enriched pathways are shown ($q < 0.05$).

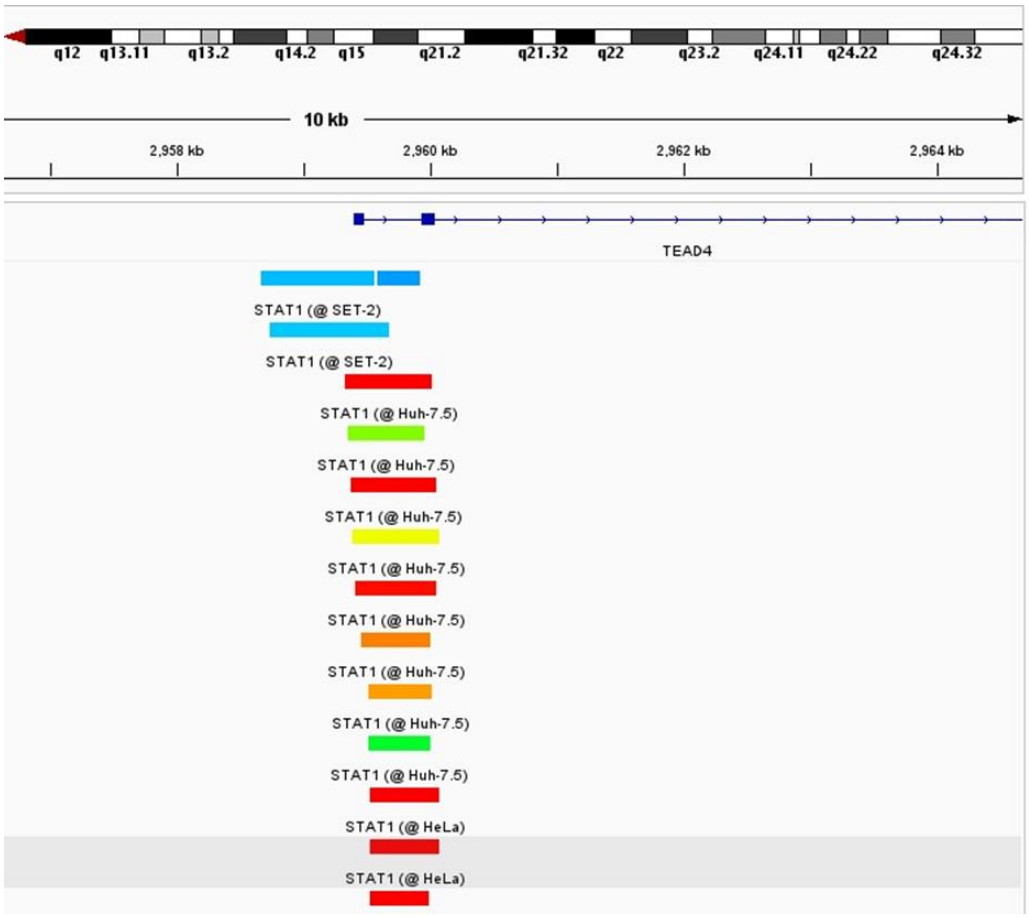


Figure S2. STAT1 binding at the TEAD4 promoter. Publicly available ChIP-seq data from ChIP-Atlas showing STAT1 binding at the TEAD4 promoter in IFN-γ-stimulated SET-2, HeLa, and Huh-7 cells.

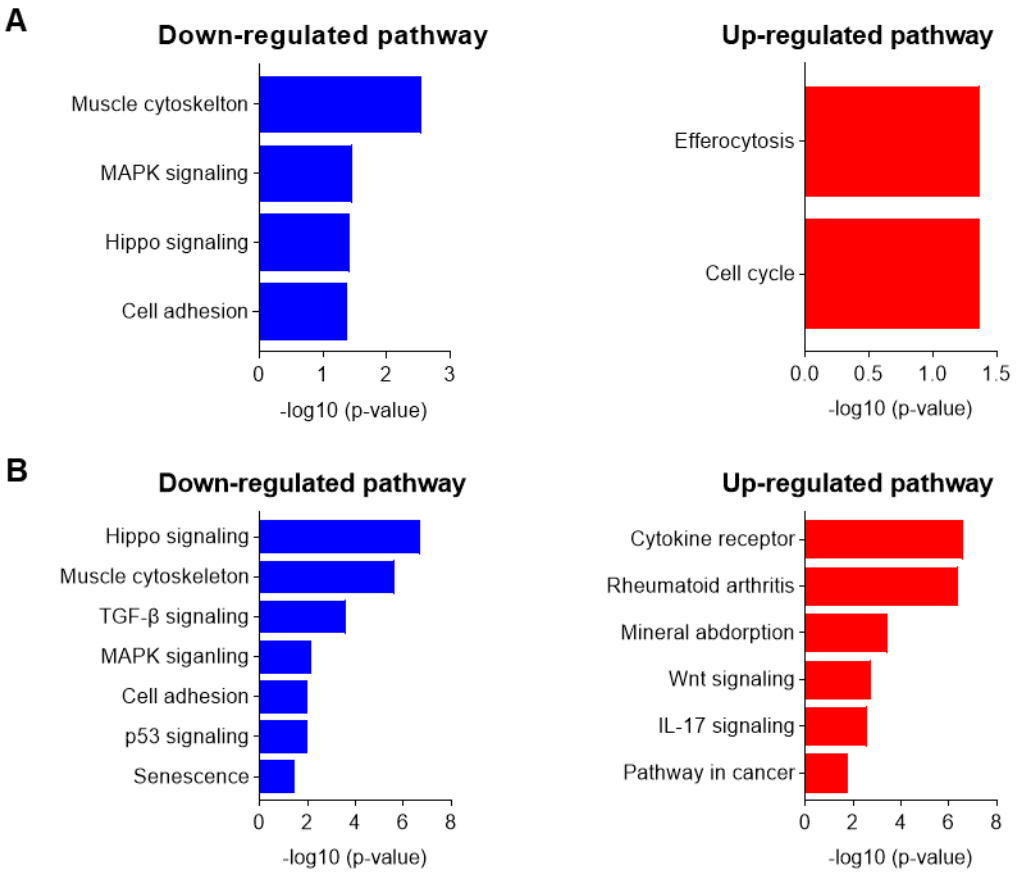


Figure S3. Transcriptomic analyses following TEAD or YAP/TAZ knockdown in RASFs. (A, B) KEGG pathway enrichment analysis of differentially expressed genes (DEGs) in 4mix-stimulated RASFs transfected with siTEAD1/3/4 (A) or siYAP/TAZ (B) compared with control siRNA (siCtrl). The top enriched pathways are shown ($P < 0.05$).

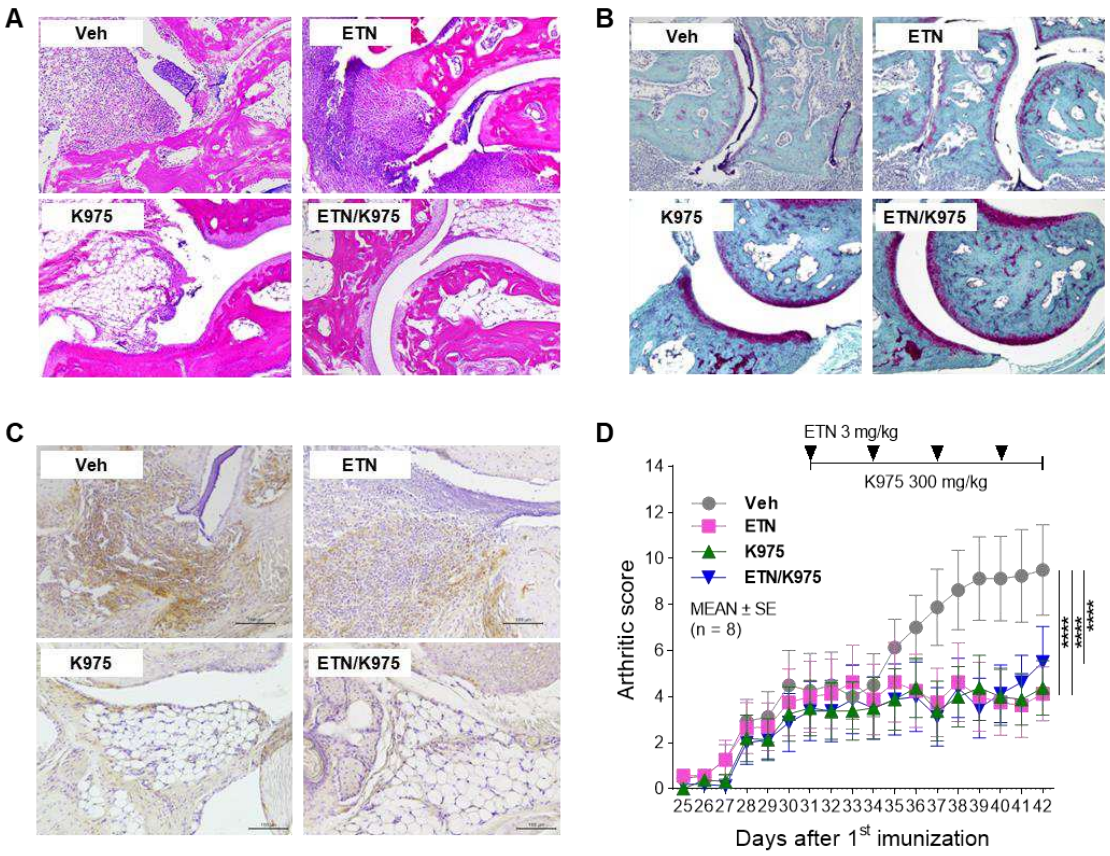


Figure S4. Histological and therapeutic evaluation of collagen-induced arthritis following pan-TEAD inhibition and TNF blockade. (A) Higher-magnification hematoxylin and eosin (H&E) images corresponding to Figure 5*E* used for histological scoring of synovial inflammation and bone erosion. (B) Representative Safranin *O* staining of articular cartilage. (C) Immunohistochemical staining of fibroblast activation protein (FAP) in hind paws. FAP staining intensity was scored as 0 (none), 1 (weak), or 2 (strong). (D) Therapeutic collagen-induced arthritis model. Treatment was initiated on day 31 after disease onset with K975 (300 mg/kg) with or without etanercept (ETN; 3 mg/kg, intraperitoneally administered on days 31, 34, 37, and 40). Data are presented as mean ± SEM (n = 6 in C; n = 8 in D). Statistical significance was determined by one-way ANOVA followed by Dunnett's multiple-comparison test (C) or two-way ANOVA followed by Bonferroni's multiple-comparison test (D). $P < 0.05$; $P < 0.0001$.

Table S1. Clinical information of RA and OA patients for synovial tissue samples included in this study. Anti-citrullinated protein/peptide antibody (ACPA), Biological disease-modifying antirheumatic drug (bDMARD), C-reactive protein (CRP), Conventional synthetic disease-modifying antirheumatic drug (csDMARD), Rheumatoid factor (RF).

Clinical data	RA	OA
Number (M/F)	8 (3/5)	3 (0/3)
Age mean (range)	77.6 (71-84)	69.3 (57-79)
ACPA (+/-)	(5/3)	(0/3)
RF (+/-)	(6/2)	(0/3)
CRP (mg/dl), mean ± SD	2.6 ± 2.3	-
Disease duration (years), mean ± SD	9.3 ± 9.8	-
Medication	csDMARD (7), bDMARD (5)	-

Table S2. Primer sequences used for qPCR analysis.

Gene	Forward	Reverse
Human GAPDH	5’-GTCTCCTCTGACTTCAACAGCG-3’	5’-ACCACCCTGTTGCTGTAGCCAA-3’
Human TEAD1	5’-ATGCCAACCATTCTTACAGTGAC-3’	5’-ACAGTTCCTTTAAGCCACCTTTC-3’
Human TEAD3	5’-TGGACCCTCTCAGGACATCAA-3’	5’-CCAGGGGCTCATAACTGCTG-3’
Human TEAD4	5’-GGACACTACTCTTACCGCATCC-3’	5’-TCAAAGACATAGGCAATGCACA-3’
Human IRF1	5’-GCAGCTACACAGTTCCAGG-3’	5’-GTCCTCAGGTAATTTCCCTTCCT-3’
Human IL6	5’-TCGACGGCATCTCAGCCCTGAG-3’	5’-AGGTTGTTTTCTGCCAGTGCCTCTT-3’
Human CCL2	5’-ATCACCAGCAGCAAGTGTC-3’	5’-AGGTGGTCCATGGAATCCTG-3’
Human ANKRD1	5’-AGCGCCCGAGATAAGTTGCT-3’	5’-CACCAGATCCATCGGCGTCT-3’
Human CCN1	5’-AGCCTCGCATCCTATACAACC-3’	5’-TTCTTTCACAAGGCGGCACTC-3’
Human CTGF	5’-GCAGGCTAGAGAAGCAGAGC-3’	5’-ATGTCTTCATGCTGGTGCAG-3’
Human COMP	5’- GCAGACAAGGTGGTAGACAAGA-3’	5’-GCCTGGGTCGCTGTTCATT-3’
Human PRELP	5’-CAGCCAACAAGACGACCAAGA-3’	5’-CAGTCAGGGAAGATAGATGGAGG-3’
Human TGFBR2	5’-ACCACTGGGAGTTGCCATATCT-3’	5’-TCCCAGGTTGAACTCAGCTTCT-3’
Human IL1R1	5’-AGAGGAAAACAAACCCACAAGG-3’	5’- CTGGCCGGTGACATTACAGAT-3’

Supplementary Files

This is a list of supplementary files associated with this preprint. Click to download.

- FulluncroppedGelsandBlotsimages.pdf